ELSEVIER

Contents lists available at ScienceDirect

Colloids and Surfaces B: Biointerfaces

journal homepage: www.elsevier.com/locate/colsurfb





Invasiveness modulation of glioma cells by copper complex-loaded nanoarchitectures

Agata Zamborlin ^{a,b,1}, Francesca Pagliari ^c, Maria Laura Ermini ^a, Valentina Frusca ^{a,d}, Daniel García-Calderón ^{c,g}, Luca Tirinato ^{c,e}, Stefania Volante ^f, Giulio Bresciani ^f, Fabio Marchetti ^f, Joao Seco ^{c,g,*}, Valerio Voliani ^{a,h,**}

- ^a Center for Nanotechnology Innovation@ NEST, Istituto Italiano di Tecnologia, Piazza San Silvestro, 12, Pisa 56127, Italy
- ^b NEST-Scuola Normale Superiore, Piazza San Silvestro, 12, Pisa 56127, Italy
- ^c Division of BioMedical Physics in Radiation Oncology, German Cancer Research Center, Heidelberg 69120, Germany
- d Scuola Superiore Sant'Anna, Piazza Martiri della Libertà, 33, Pisa 56127, Italy
- ^e Department of Medical and Surgical Science, University Magna Graecia, Catanzaro 88100, Italy
- f Department of Chemistry and Industrial Chemistry, University of Pisa, Via Moruzzi 13, Pisa 56124, Italy
- g Department of Physics and Astronomy, Heidelberg University, Im Neuenheimer Feld 227, Heidelberg 69120, Germany
- h Department of Pharmacy, School of Medical and Pharmaceutical Sciences, University of Genoa, Viale Cembrano, 4, Genoa 16148, Italy

ARTICLE INFO

Keywords: Gold nanoparticles Copper complex Metastasis Invasiveness Neuroglioma Epithelial-to-mesenchymal transition

ABSTRACT

Among the tumors with the highest lethality, gliomas are primary brain tumors associated with common recurrence inclined to metastasize along the neuraxis and occasionally out of the central nervous system. Even though metastasis is the main responsible for death in oncological patients, few dedicated treatments are approved. Therefore, the establishment of effective anti-metastasis agents is the final frontier in cancer research. Interestingly, some copper complexes have demonstrated promising efficacy as antimetastatic agents, but they may cause off-site effects such as the alteration of copper homeostasis in healthy tissues. Thus, the incorporation of copper-based antimetastatic agents in rationally designed nano-architectures can increase the treatment localization reducing the side effects. Here, copper complex loaded hybrid nano-architectures (CuLNAs) are presented and employed to assess the impact of an intracellular copper source on glioma cell invasiveness. The novel CuLNAs are fully characterized and exploited for cell migration modulation in a glioma cell line. The results demonstrate that CuLNAs significantly reduce cell migration without impairing cell proliferation compared to standard gold and copper NAs. A concomitant antimigratory-like regulation of the epithelial-tomesenchymal transition genes confirmed these results, as the gene encoding for the epithelial protein E-cadherin was upregulated and the other explored mesenchymal genes were downregulated. These findings, together with the intrinsic behaviors of NAs, demonstrate that the inclusion of metal complexes in the nano-architectures is a promising approach for the composition of a family of agents with antimetastatic activity.

1. Introduction

Brain tumors are the most frequent pediatric neoplasms and account for most of cancer deaths [1]. In particular, gliomas represent approximately 50% of all tumors in this age range, while decreasing to 30% during adolescence [1]. In United States, even though primary malignant brain tumors are quite scarce during adulthood (roughly around

1 % of incidence), they are characterized by high fatality rate [2]. Gliomas are brain cancers formed by non-neural cells called glial cells, and they are associated with poor prognosis and progressive cognitive and functional impairment [3]. Therapeutic approaches for gliomas include surgical resection, when possible, or radiotherapy, and chemotherapy [4]. In glioma treatment, radiation therapy is exploited to locally control the tumor volume reducing the possible neurotoxicity, in order to delay

^{*} Corresponding author at: Division of BioMedical Physics in Radiation Oncology, German Cancer Research Center, Heidelberg 69120, Germany.

^{**} Corresponding author at: Department of Pharmacy, School of Medical and Pharmaceutical Sciences, University of Genoa, Viale Cembrano, 4, Genoa 16148, Italy. E-mail addresses: j.seco@dkfz-heidelberg.de (J. Seco), valerio.voliani@unige.it (V. Voliani).

¹ Current affiliation: Ghent Research Group on Nanomedicines, Laboratory of General Biochemistry and Physical Pharmacy, Faculty of Pharmaceutical Sciences, Department of Pharmaceutics, Ghent University, Ottergemsesteenweg 460, 9000 Ghent, Belgium

neurological impairment and improving survival [4]. Radiotherapy is normally used when tumor position and diffusivity do not allow a safe surgical removal [5]. Moreover, even when surgical resection is a viable option, radiotherapy may follow to treat the residual areas around the tumor mass within 3–5 weeks from resection [4]. Nevertheless, recurrence can also happen in 90 % of patients, typically within 2 cm of the resected tumor area which can be invaded by residual cancer cells [3,6]. Surgery and treatment resistance strategies may stimulate cell migration and relapses as invasive malignant gliomas tend to spread along the neuraxis through the extracellular space in brain [3,7]. High-grade gliomas hardly metastasize out the central nervous system (less than 2 % of cases) especially without surgical disruption of dura and calvarium. When glioma metastases exit the central nervous system, lungs, lymph nodes, bones, and liver are the most targeted organs [6].

Invasion and metastasis are cancer hallmarks associated with recurrence and poor prognosis [8]. The mechanisms leading to migration of cancer cells are related to the epithelial-to-mesenchymal transition (EMT) [9]. EMT is consequence of the genome instability characterizing cancer cells, which causes the loss of epithelial features, and the gaining of mesenchymal properties associated with migrating cells [10]. Moreover, the invasive tumor cells actively synthetize extracellular proteolytic enzymes to ease their movement, e.g., matrix metalloproteinases (MMP), heparinase, and plasmin [3]. Due to its role in metastasis, EMT is a promising target for antimetastatic treatments [11,12]. Indeed, EMT reversion may prevent the development of metastasis, reducing cancer invasion, and improving drug sensitivity [13,14]. At a molecular level, epithelial genes are downregulated, as CDH-1 encoding for E-cadherin, whereas mesenchymal genes encoding for Vimentin and N-cadherin are activated. Twist, Snail, Zeb, and Slug are the primary EMT-transcriptional factors (EMT-TFs) that can regulate matrix metalloproteinases (MMPs), and whose overexpression stimulates cell migration [10]. SNAI1 encodes for Snail protein that silences the transcription of CDH-1 while upregulating Vimentin [13]. The transcriptional repression of CDH-1 gene by SNAI1 and ZEB reduces the expression of E-cadherin, causing loss of epithelial features as cell adhesion while becoming mesenchymal-like, hence able to migrate. In addition, Zeb promotes the transcription of Vimentin and N-cadherin. Twist contrasts cell adhesion and stimulates cell mobility by suppressing E-cadherin and promoting N-cadherin expression (cadherin switch) [13,

Nowadays, no specific chemo-therapeutical approaches for brain cancer metastasis are available, despite several nanoparticle-based strategies are currently undergoing clinical trials [16]. Interestingly, promising antimetastatic agents for some neoplasms are metal-based compounds, e.g., copper complexes [17,18]. Cu complexes are deemed to non-covalently bind DNA, to interact with Topoisomerase I-II, and proteasome, suggesting anti-angiogenic/-metastatic/-inflammatory properties, as well as MMP2 inhibition [19]. On this regard, the biological safety of copper is still uncertain, especially considering the affinity of Cu⁺ and Cu²⁺ for methionine and cysteine or aspartic/glutamic acid and histidine residues in proteins, respectively [20]. Nanostructured copper may confine the side effects due to systemic distribution of copper complexes while increasing the local effects on DNA damage and apoptosis on cancer cells [20]. Recently, we investigated the biosafety and the role of copper ultrasmall-in-nano architectures (CuNAs) in delaying the metastatic process in in vitro and chorioallantoic membrane (CAM) models of pancreatic ductal adenocarcinoma [21]. In CAMs, CuNAs upregulated the expression of E-cadherin encoding gene and protein in the primary tumors, while reducing the number of cancer cells in distal sites of the CAM model. On this basis, we extended the investigation to glioma, which can be affected by variations of copper content, and to a novel intracellular source of copper.

Here, copper complex loaded hybrid nano-architectures (CuLNAs) are successfully developed, adding a novel member to the family of the ultrasmall-in-nano architectures (NAs). NAs are biodegradable and non-persistent nanoplatforms already employed in preclinical cancer

research [22,23]. CuLNAs were successfully synthetized and characterized, and their effect on H4 glioma cells was evaluated in terms of cytotoxicity and anti-invasiveness. H4 cells were selected as 2D glioma model since a progenitor of CuL showed interesting antimigratory properties (retained even following irradiation) on this cells line [17]. To assess wheter the anti-invasiveness property of copper may be affected by its chemical source, CuLNAs activity was compared with AuNAs and CuNAs as controls. Our quantitative investigation underlined an enhanced antimigratory effect of CuLNAs compared to the two nanostructured metals alone, supporting further efforts toward the composition of a family of anti-metastatic agents for gliomas based on hybrid nano-architectures.

2. Materials and methods

2.1. Synthesis of copper complex (CuL)

Copper(II) chloride dihydrate (99 %+) was purchased from Strem Chemicals (Newburyport, MA, USA), other reactants and solvents were obtained from Merck (Darmstadt, Germany) or TCI Chemicals (Tokyo, Japan) and were of the highest purity available. 2-(((Pyridin-2vlmethyl)amino)methyl)phenol (L1) [24] and 2-(oxiran-2-vlmethyl) isoindoline-1,3-dione (L2) [25] were prepared according to the respective literature procedures. Reactions were carried out in air with common laboratory glassware. CHN analyses were performed on a Vario MICRO cube instrument (Elementar, Lomazzo (CO), Italy). NMR spectra were recorded on JEOL YH JNM-ECZ400S or JNM-ECZ500R (JEOL USA, Inc., Peabody, MA, USA) instruments equipped with a Royal HFX broadband probe. Chemical shifts are referred to the residual solvent peaks (¹H, ¹³C). IR spectra of solid samples (650–4000 cm⁻¹) were recorded on a Agilent Cary 630 FTIR spectrometer (Agilent Technologies, Santa Clara, CA, USA) equipped with a UATR sampling accessory. UV-Vis spectra were recorded on an Ultrospec 2100 Pro spectrophotometer (Biochrom US, Holliston, MA, USA) using quartz cuvettes (1 cm pathlength). IR and UV-Vis spectra were processed with Spectragryph software [26].

3. Synthesis of ligand L* (Scheme 1)

3.1. Synthesis of 2-{2-Hydroxy-3-[(2-hydroxy-benzyl)-pyridin-2-ylmethyl-amino]-propyl}-isoindole-1,3-dione (L3) [27]

In a round bottom flask, L1 (1.00 g, 4.67 mmol) and L2 (1.11 g, 5.46 mmol) were dissolved in methanol (10 mL). The resulting solution was stirred at room temperature for 96 hours (h). The obtained precipitate was isolated, washed with cold isopropanol (2 ×20 mL) and dried under vacuum. Yield 945 mg, 48 %. 1 H NMR (CDCl₃): δ /ppm = 8.55 (m, 1 H, CH_{arom}), 7.85–7.78 (m, 2 H, CH_{arom}), 7.73–7.67 (m, 2 H, CH_{arom}), 7.63 (m, 1 H, CH_{arom}), 7.22–7.16 (m, 1 H, CH_{arom}), 7.14–7.07 (m, 2 H, CH_{arom}), 6.97 (dd, 1 H, CH_{arom}), 6.79–6.67 (m, 2 H, CH_{arom}), 4.22–4.12 (m, 1 H, CH), 4.03 (d, 1 H, CH₂), 3.94 (d, 1 H, CH₂), 3.85 (d, 1 H, CH₂), 3.72–3.68 (m, 2 H, CH₂), 3.66–3.59 (m, 1 H, CH₂), 2.77–2.68 (m, 2 H, CH₂). 13 C NMR (CDCl₃): δ /ppm = 168.6 (C), 157.4 (C), 157.2 (C), 148.9 (CH), 137.3 (CH), 134.1 (3xCH), 132.1 (CH), 129.6 (CH), 129.1 (CH), 123.4 (3xCH), 122.6 (C), 122.3 (CH), 119.3 (CH), 116.8 (CH), 67.1 (CH), 58.6 (2xCH₂), 58.0 (CH₂), 42.2 (CH₂).

3.2. Synthesis of 2-{[(3-Amino-2-hydroxy-propyl)-pyridin-2-ylmethyl-amino]-methyl}-phenol (L*) [28]

In a round bottom flask, L3 (945 mg, 2.26 mmol) and hydrazine monohydrate (220 μ L, 4.52 mmol) were mixed with 10 mL of ethanol. The resulting solution was refluxed at 90°C for 3 h, during which formation of a white precipitate occurred. The mixture was cooled to room temperature, then a few drops of aqueous HCl were added. The obtained mixture was heated for 30 minutes at 80°C, afterwards the precipitate

Scheme 1. Sequential synthesis of the multidentate ligand L*.

was filtered off. The filtrate was dried under reduced pressure and subsequently dissolved in water. This solution was treated with Na₂CO₃ until pH 10.0. The organic phase was extracted with dichloromethane, then the volatiles were removed under vacuum to give an orange oil. Yield 423 mg, 65 %. Anal. calcd. for C₁₆H₂₁N₃O₂: C, 66.86; H, 7.37; N, 14.63. Found: C, 65.92; H, 7.50; N, 14.47. ¹H NMR (CDCl₃): δ /ppm = 8.57 (d, 1 H, CH_{arom}), 7.64 (m, 1 H, CH_{arom}), 7.22–7.13 (m, 3 H, CH_{arom}), 6.99 (dd, 1 H, CH_{arom}), 6.83 (m, 1 H, CH_{arom}), 6.76 (m, 1 H, CH_{arom}), 4.00 (m, 1 H, CH₂), 3.88 (d, 1 H, CH₂), 3.85 (d, 1 H, CH₂), 3.80–3.73 (m, 1 H, CH), 2.74–2.48 (m, 4 H, CH₂). ¹³C {¹H} NMR (CDCl₃): δ /ppm = 157.6 (C); 157.5 (C), 149.0 (CH); 137.1 (CH), 129.7 (CH), 129.1 (CH), 123.4 (CH), 122.7 (C), 122.6 (CH), 119.2 (CH9, 116.6 (CH), 69.5 (CH), 59.1 (CH₂), 58.3 (CH₂), 57.8 (CH₂), 45.6 (CH₂).

3.3. Synthesis of [CuL] [29]

A solution of 2-{[(3-amino-2-hydroxy-propyl)-pyridin-2-ylmethyl-amino]-methyl}-phenol (L*; 69 mg, 0.24 mmol) in methanol (3 mL) was stirred at reflux temperature for 10 minutes. Then, CuCl₂·2 H₂O (27 mg, 0.16 mmol) in methanol solution (2 mL) was added. The resulting mixture was stirred for 2 h at reflux. After cooling to room temperature, the volatiles were removed under reduced pressure and the obtained oil was treated with isopropanol, affording a dark-green solid which was separated from the liquid phase. The isolated solid was dried under vacuum. Yield 55 mg, 82 %. Anal. calcd. for C₁₆H₂₁Cl₂CuN₃O₂: C, 45.56; H, 5.02; N, 9.96. Found: C, 44.48; H, 5.08; N, 9.45. IR (solid state): 0/cm⁻¹ = 3110s-br, 2927w, 2861w, 1638w, 1610 m, 1596w, 1507w, 1482w, 1450 m, 1392w, 1354w, 1299w, 1262 m, 1188w, 1154w, 1052 m, 1030 m, 984w, 946w, 756vs, 733 s, 698 m, 657 s. UV-Vis (MeOH, ca. 2•10⁻⁴ M): $\lambda_{max} = 263$ nm.

3.4. Synthesis of AuNAs and of copper complex-gold nano-architectures (CuLNAs)

- a. Synthesis of gold seeds. Ultrasmall gold nanoparticles (Au USNPs, 3 nm diameter) were prepared according to the following procedure. 10 μL of poly(sodium 4-styrenesulfonate) (PSS, 70 kDa, 30 % in water; Sigma-Aldrich, Darmstadt, Germany, #527483) and 200 μL of HAuCl4 aqueous solution (29.4 mM) (Alfa Aesar, Ward Hill, MA, USA, #36400) were added to 20 mL of Milli-Q® water. 200 μL of NaBH4 aqueous solution (211 mM) (Sigma-Aldrich, #452882) was added while vigorously stirring, and the solution was mixed for other 2 minutes. After 10 minutes, the suspension appeared brilliant orange. For the synthesis of CuLNAs, 85 μL of a 10 mg/mL CuL solution was added under gentle stirring and the reaction mixture was allowed to turn darker.
- b. Synthesis of gold arrays. To form the arrays, 75 μ L of poly(L-lysine) (PL, 15–30 kDa, 40 mg/mL in Milli-Q®; Sigma-Aldrich, #7890) was slowly dropped to the reaction mixture, which was stirred for 20 minutes at room temperature. A 3-minute centrifugation at 17092 rcf allowed to collect the arrays, which were then resuspended in 2 mL of Milli-Q® water.

c. Synthesis of nanoarchitectures. The silica shell was formed according to a modified Stöber reaction. The sonicated array suspension was added to 70 mL of absolute ethanol (Sigma-Aldrich, #24105) previously added of 40 µL of tetraethyl orthosilicate (TEOS, 98 %; Sigma-Aldrich, #131903) and 2.4 mL of ammonium hydroxide (Sigma-Aldrich, #221228). The suspension was mildly shaken for 3.5 h at room temperature. A 30-minute centrifugation at 3220 rcf allowed to collect the so-formed NAs, which were resuspended in 2 mL of ethanol, and washed once with ethanol and once with water to remove unreacted reagents. A short spin (14 seconds at 14462 rcf) was employed to discard the bigger NAs, and the collected supernatant was further washed in ethanol and finally stored in 1 mL of ethanol at -20°C.

3.5. Synthesis of CuNAs

The synthesis of CuNAs has been described elsewhere [30]. Briefly, copper USNPs (<2 nm diameter) were produced by reduction of CuSO₄ (25 mM; Sigma-Aldrich, #209198) using reduced L-glutathione solution (100 mM; Sigma-Aldrich, #G4251) and sodium borohydride (211 mM; Sigma-Aldrich, #452882). Cu USNPs were embedded in a polymeric matrix of PL and PSS. The so-called arrays were then shielded by a silica shell obtained via a modified Stöber reaction using dimethylamine (DMA, 40 % stock, 428 mg/mL; Alfa Aesar, #31458) as catalyzer, thus forming CuNAs of around 150 nm in size. CuNAs were washed twice in ethanol, short-spun, and then stored in ethanol at -20° C.

3.6. Characterization of CuLNAs

a. Dynamic Light Scattering (DLS) and Zeta-potential measurements. 100 μL of CuLNAs suspension was spun at 14462 rcf for 3 minutes to remove ethanol. NAs were resuspended in 300 μL of 1X PBS pH 7.4 and dropped in a 1 mL quartz cuvette for DLS. The hydrodynamic diameter of CuLNAs was measured at 25°C using a Malvern Zetasizer Nano ZS90 (Malvern Panalytical Ltd., Malvern, UK) equipped with a red laser (633 nm) at a fixed angle (90°). The results derived from three consecutive measurements of 10 runs of 10 seconds each using Zetasizer Software version 7.13. Values were reported as zeta average \pm standard deviation (nm).

The Zeta-potential of CuLNAs was measured diluting the suspension to 1 mL using 1X PBS pH 7.4 and placing it into a DTS 1070 standard capillary cell. The results were reported as zeta potential \pm standard deviation (mV).

- b. Electron Microscopy. Transmission electron microscopy (TEM) images were captured with a ZEISS Libra 120 (ZEISS, Oberkochen, Germany), operated at 120 kV accelerating voltage. CuLNAs alcoholic suspension was placed on 300-mesh carbon-coated copper grids and the images were collected once dried. ImageJ software was used to analyze TEM images, measuring particle diameters and silica shell size on approximately 100 NAs.
- c. UV-Vis spectrophotometry. 5 μ L of CuLNAs suspension was spun at 14462 rcf for 3 minutes to remove ethanol and resuspend NAs sample in 5 μ L of 1X PBS pH 7.4. 3 μ L of the resuspended CuLNAs

was dropped on the microplate of a Mettler Toledo UV5 Nano Spectrophotometer (Mettler Toledo, Columbus, OH, USA) and the analysis was performed applying a 0.105 mm path length. Spectra were analyzed using OriginLab software.

d. Inductively Coupled Plasma-Mass Spectrometry (ICP-MS) Analysis. The quantification of gold and copper in CuLNAs, AuNAs, and CuNAs was operated using an ICP-MS Agilent 7700 (Agilent Technologies, Santa Clara, CA, USA). Pre-digestion of samples was induced with aqua regia made of 3:1 hydrochloric acid:nitric acid (hydrochloric acid: 34-37 % in HCl, TraceMetal Grade; Thermo Fisher Scientific, Waltham, MA, USA, #A508-P500; nitric acid: 65 % Suprapur®; Sigma-Aldrich, #1.00441), and samples were then stirred at 200°C under a microwave irradiation protocol using CEM Discover SP-D digestion microwave (CEM, Matthews, NC, USA). The solution was diluted adding 3 mL of 3 % nitric acid solution, and the quantification of metal content was performed using standard calibration curves (gold standard 1000 ppm: Absolute Standards, inc., #56079; copper standard 1000 ppm: Merck KGaA, #1.70314.0100). As an internal standard, 10 ppm Hg (Mercury standard for ICP TraceCERT®, 10000 ppm; Sigma-Aldrich, #75111) in 3 % nitric acid solution was used.

3.6.1. Cell culture

Human brain neuroglioma (H4) cells were purchased from ATCC (Manassas, VA, USA). H4 cells were cultured in Dulbecco's Modified Eagle's Medium (DMEM) (GibcoTM, Thermo Fisher Scientific, #11995065) with 10 % Fetal Bovine Serum (FBS; GibcoTM, Thermo Fisher Scientific, #10500064) and 1 % penicillin/streptomycin (GibcoTM, Thermo Fisher Scientific, #15140122) (hence defined as complete medium) at 37°C and 5 % CO₂. Cells were washed with 1X DPBS (GibcoTM, Thermo Fisher Scientific, #14190169) and detached using 1X Tryple Express Enzyme (Thermo Fisher Scientific, #12604013). Cells were routinely tested for the absence of Mycoplasma by using the EZ-PCR Mycoplasma Detection Kit (Biological Industries, Beit HaEmek, Israel; #20–700–20).

3.6.2. Cell viability assay

H4 cells viability assays were performed using alamarBlueTM Cell Viability Reagent (Thermo Fisher Scientific, #DAL1100). H4 cells were seeded at a density of 7.0×10^3 cells/well in a 96-well black polystyrene microplate (Corning Incorporated, Corning, NY, USA, #353376) and incubated overnight at 37°C. The following day, the medium was removed, cells were washed twice with DPBS, and NAs treatments were applied (100 μ L/well, 0.5 μ g/mL Cu and 5 μ g/mL Au per well). NAs were prepared discarding ethanol through spinning at 14462 rcf for 3 minutes and resuspending them in complete medium. After 24 h of incubation, the treatments were withdrawn, and cells were washed twice with DPBS. Then, 100 µL of a 10 % solution of alamarBlue™ in complete medium was added to each well. The plate was shielded from light with aluminum foil, and incubated for 2 h at 37°C. The plate was read using a CLARIOstar® microplate reader (BMG LABTECH GmbH, Offenburg, Germany) for fluorescence detection (excitation: 557-15 nm; emission 597-14 nm). Results are presented as % viability over the viability of the non-treated cells (control).

3.6.3. Cell migration assay

Wound healing assay was employed to investigate the effect of NAs on H4 cell migration. Briefly, 7.0×10^3 cells/well were seeded into culture-insert 4-well plates (Ibidi, Grafelfing, Germany, #80466) and incubated overnight at 37° C. The treatments were applied to each well of the plate (0.5 µg/mL Cu and 5 µg/mL Au in NAs per well) following resuspension of NAs in complete medium. After 24 h of incubation at 37° C, cells were confluent along the walls of the insert. The treatments were washed with DPBS, fresh complete medium was added, and finally the insert was removed. The cell migration was followed and imaged

every 6 h at 10X Magnification for a total of 72 h after the treatment application using an Eclipse Ts2 optical microscope (Nikon Corporation, Tokyo, Japan). The size of the gap was measured using ImageJ software. The areas of the gaps were measured at every time point and then normalized over time zero (meaning when the insert was removed) and then again to the control (non-treated cells).

3.6.4. Cell counting assay

To evaluate whether the effect on cell migration was due to a reduced cell proliferation, cells were counted at significative time points after the treatment application. Cells were seeded at a density of 7.0×10^3 cells/ well in 96-well flat-bottomed white plates and incubated at 37°C for 24 h. The next day, cells were washed twice with DPBS and treated with $0.5 \,\mu g/mL$ Cu and $5 \,\mu g/mL$ Au in NAs per well (100 μL per well). NAs were prepared discarding ethanol through spinning at 14462 rcf for 3 minutes and resuspending them in complete medium. After 24 h, the treatments were removed, cells were washed twice with DPBS and added of fresh complete medium. For cell fixation, at 24, 48, and 72 h after the treatment application, cells were washed with 100 µL of 1X PBS with Ca²⁺ and Mg²⁺ (Thermo Fisher Scientific, #14080055), and fixed using 50 µL of cold 4 % paraformaldehyde (PFA; Pierce 16 % Formaldehyde in DPBS, Thermo Fisher Scientific, #28908) for 15 minutes at room temperature. PFA was then removed via a double washing in PBS with Ca²⁺ and Mg²⁺. For nuclei staining, 100 μL of a 1 μg/mL solution of Hoechst 33342 dye (Thermo Fisher Scientific, #62249) was applied at room temperature for 20 minutes while protected from light. After the incubation, cells were washed twice with 100 µL of PBS with Ca²⁺ and Mg²⁺. 100 µL of PBS with Ca²⁺ and Mg²⁺ was added to support image acquisition. Images were obtained with an Eclipse Ti2 inverted microscope (Nikon) and analyzed using ImageJ software. A specific Macro was designed within ImageJ to count the stained nuclei, and the cell number was normalized to the control according to the following formula: Normalized number of cells = $\frac{\text{Number of cells sample}}{\text{Number of cells control}}$

3.6.5. RNA extraction

H4 cells were seeded at the density of 2.1×10^5 cells/well in a 6-well plate and incubated for 24 h at $37^\circ C$. The following day, cells were washed with DPBS and treated with 0.5 µg/mL Cu and 5 µg/mL Au in NAs per well (1 mL/well). NAs were prepared as previously described, and cells were incubated with treatments for 24 h. 48, 54, or 72 h after the treatment application, cells were detached using 500 µL 1X Tryple Express Enzyme. After centrifuging, cells were counted and approximately 1.0×10^6 cells were used for RNA extraction by using the High Pure RNA isolation kit (Roche, Basel, Switzerland, #11828665001) according to the manufacturer's instructions. Total RNA was resuspended in 50 µL of RNAse-free water (Thermo Fisher Scientific, #15815408) and quantified using a Nanodrop ND-1000 (Thermo Fisher Scientific). RNA quality and extraction efficiency was evaluated through agarose gel electrophoresis.

3.6.6. cDNA synthesis

 $1\,\mu g$ of total RNA was reverse transcribed according to the instructions of the RT2 first strand kit (Qiagen, Hilden, Germany, #330404). cDNA was suspended with nuclease-free water at the final concentration of 5 ng/µL (200 µL).

3.6.7. Real Time quantitative PCR (RT-qPCR) analysis

cDNA was used to evaluate gene expression by real-time PCR (RT-qPCR). 25 ng of cDNA was amplified in 15 μL of a reaction mix containing Power SYBR® Green PCR Master Mix (Thermo Fisher Scientific, #4368706), 20 pmol of each primer pair (listed in Table 1), and nuclease-free water. The internal control was the human RPLP0 cDNA fragment. The temperature profile used for the amplification consisted of one cycle at $95^{\circ}C$ for 10 minutes, followed by 40 cycles at $95^{\circ}C$ for 15 seconds and $60^{\circ}C$ for 1 minute. Data were analyzed using ABI

Table 1List of primers for RT-qPCR.

| Gene | Forward Primer (5'→3') | Reverse Primer (5'→3') CAGACACTGGCAACATTGC | |
|------------|----------------------------|---|--|
| RPLP0 | GGTCATCCAGCAGGTGTTC | | |
| E-Cadherin | ACAGGAACACAGGAGTCATC | TGTTGCTGTTGTGCTTAACC | |
| Snail | TCCAGAGTTTACCTTCCAGC | AGAGTCCCAGATGAGCATTG | |
| Vimentin | GATGTTGACAATGCGTCTCTG | TGTTCCTGAATCTGAGCCTG | |
| Twist | CTTCCTCTACCAGGTCCTC | CAGACCGAGAAGGCGTAG | |
| N-Cadherin | TGCCCCTCAAGTGTTACCTC | CACCATTAAGCCGAGTGATG | |
| MMP2 | CCTGAACACCTTCTATGGCTG | CTGGTCAAGATCACCTGTCTG | |
| MMP9 | CGTCTTCCCCTTCACTTTCC | AGGATGTCATAGGTCACGTAG | |
| Zeb1 | GACCACAGATACGGCAAAAG | GTAAAGGGGTTGAACAGTTGA | |
| Slug | TGCCTGTCATACCACAACCA | GACTCACTCGCCCCAAAGA | |
| c-Myc | GGG AGG AGA CAT GGT GAA CC | AGA AGC CGC TCC ACA TAC AG | |
| SOD1 | GCAGATGACTTGGGCAAAGG | TGGGCGATCCCAATTACACC | |

7900HT Real-Time PCR System (Thermo Fisher Scientific). The gene expression was normalized to the internal control gene and calculated according to the $\Delta\Delta C_t$ method [31].

3.6.8. Statistics

Statistical analysis was performed using GraphPad Prism 7 software. P-values below 0.05 were considered statistically significant (*p<0.05 **p<0.01 ****p<0.001 ****p<0.0001). Unless differently stated, two-way ANOVA with Tukey's or Dunnet's multiple comparison test was applied when comparing among treatments or between treatment and control condition, respectively.

4. Results and discussion

The multidentate N,O-ligand 2-{[(3-amino-2-hydroxy-propyl)-pyridin-2-ylmethyl-amino]-methyl}-phenol (L*), containing one pyridyl, two hydroxyl and one primary amine groups, was prepared according to a multistep procedure. Then, L* was allowed to react with copper(II) dichloride (using an approximately L*/Cu molar ratio of 1.5), leading after work-up to a presumable mixture of isomers with composition $CuCl_2 \cdot L^*$ (abbreviated as CuL). We did not detect any release of HCl, thus ruling out the possibility of OH/NH_2 moieties undergoing activation upon coordination [32,33]. The isolated material (a dark-green solid) was characterized by spectroscopic techniques and CHN elemental analysis. Analogous $CuCl_2$ adducts with strictly related N, O-ligands (coordination number of copper = 5) were previously

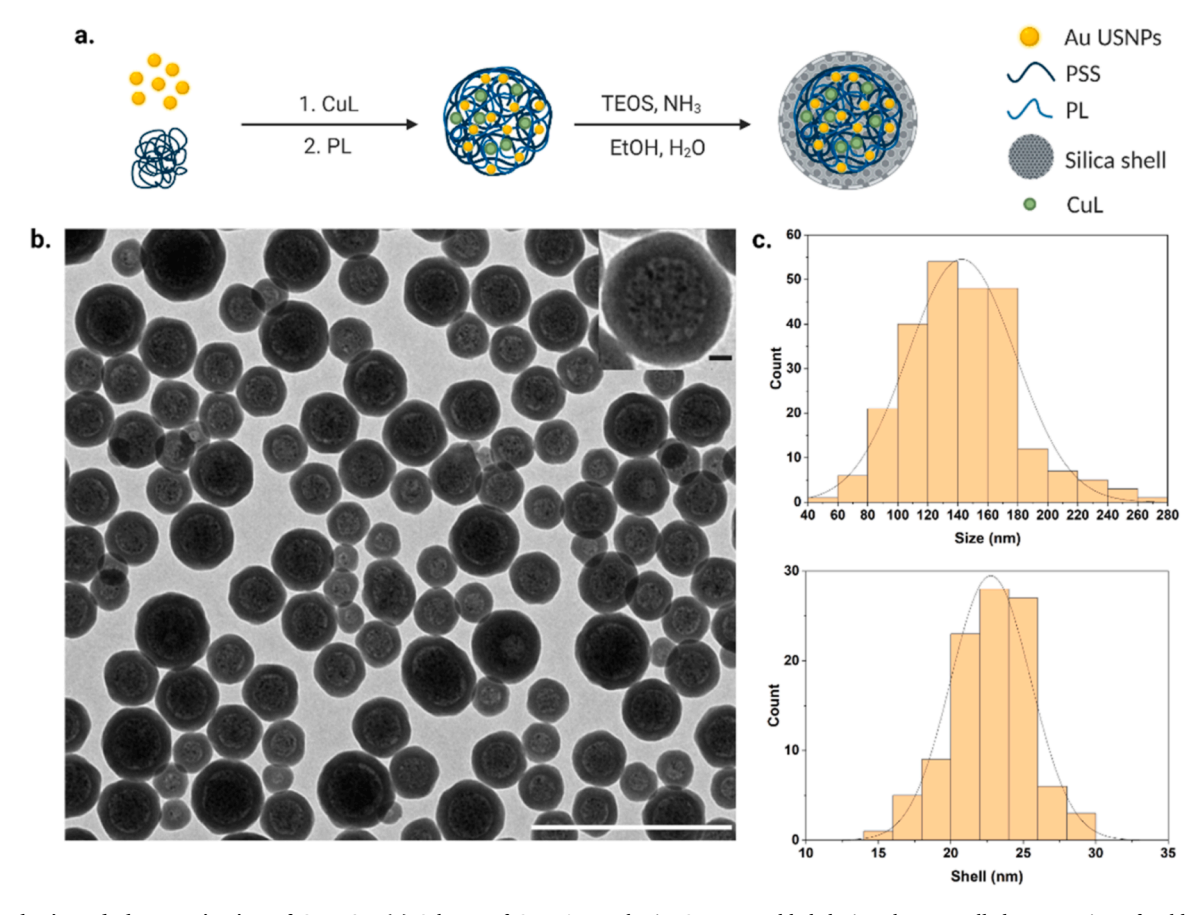


Fig. 1. Synthesis and characterization of CuLNAs. (a) Scheme of CuLNAs synthesis. CuL was added during the controlled aggregation of gold seeds in the polymeric matrix. The inner core was then embedded in a silica shell. (b) Wide-area TEM of CuLNAs. Scale bar: 500 nm. The inset is a zoom on a single nanoarchitecture. Scale bar: 20 nm. (c) Size distribution of CuLNAs diameter (upper) and silica shell thickness (bottom) calculated on at least 100 CuLNAs visualized with TEM. CuLNAs diameter and shell thickness were analyed using ImageJ.

investigated in vitro and in vivo as effective antileukemia agents [34].

The systemic biodistribution of small chemical entities can be partially reduced and targeted toward organs of interest by entrapping them in nanomaterials [35]. For this reason, we entrapped CuL in gold ultrasmall-in-nano architectures (NAs), thus forming a novel nanoplatform called here CuLNAs. NAs are biodegradable silica nano-capsules that contain ultrasmall metal nanoparticles (USNPs) of 3 nm in size (Au) or <2 nm (Cu), entrapped in a polymeric matrix [30,36]. NAs combine the plasmon features of nanostructured noble metals with a hydrodynamic diameter below the glomerular cut-off. Indeed, previous investigations showed that NAs can be administered intravenously or intranasally avoiding metal persistence, hence shifting the paradigm in translational research [37–39]. CuLNAs were obtained by adding CuL to the reaction mixture prior to forming the polymeric arrays (Fig. 1) and by following standard operative procedures (SOPs) [40]. The hydrodynamic diameter and zeta potential of CuLNAs were measured using Dynamic Light Scattering (DLS), whereas the size and shell of CuLNAs were assessed through Transmission Electron Microscopy (TEM) imaging. The values obtained for CuLNAs were comparable to the ones of AuNAs and CuNAs supporting the versatility of the SOPs (Table 2) [30, 41]. UV-Vis spectroscopy analysis of CuLNAs in PBS confirmed the plasmon absorbance in the same region of AuNAs around 520 nm (Figure S1). The metal content was evaluated using Inductively Coupled Plasma-Mass Spectrometry (ICP-MS), showing a Cu/Au mol ratio of 29 %. Overall, the introduction of copper complexes within the inner core of NAs did not affect their external and physical features, allowing a reliable comparison of the impact of the entities contained in NAs on bio-medical applications.

The in vitro anti-invasiveness effect of CuLNAs was compared to nanostructured gold and copper, provided as AuNAs and CuNAs, respectively. In particular, AuNAs highlight the effect of the copper complex while CuNAs indicate whether the source of copper ions modifies the overall antimetastatic behavior. Indeed, when dissolved and oxidized in physiological fluids, the copper seeds embedded in CuNAs may behave similarly to copper provided as CuL, and the potential different effects between CuLNAs and CuNAs can be ascribable to the complex ligands and Au USNPs [21]. H4 glioma cells were employed as in vitro 2D glioma model since a progenitor of CuL showed interesting antimigratory properties (retained even following irradiation) on this cell line. Indeed, even though gliomas are known for their reduced tendency to migrate outside the central nervous system, cancer cells may migrate to other areas of the brain worsening the prognosis [3]. Moreover, H4 cells showed the ability to invade the surrounding Matrigel® when organized in spheroids, supporting the employment of this cell line for anti-invasiveness studies [17].

From previous works on NAs as antimetastatic agents on a 2D model of a pancreatic ductal adenocarcinoma cell line, CuNAs and AuNAs resulted non-toxic while exerting mild antimigratory tendency at 0.5 $\mu g/mL$ and 5 $\mu g/mL$ for Cu and Au, respectively [21]. Therefore, we investigated the toxicity of CuLNAs, AuNAs, and CuNAs on H4 glioma cells at similar metal concentrations (Fig. 2a). The molar ratio between gold and copper found in CuLNAs was maintained in cellular studies between the different treatments to examine the effect of each metal in CuLNAs. As expected, the tested concentrations were non-toxic for cells after a 24 h-treatment and therefore they were further used to

Table 2Comparison of the principal features of the different types of NAs.

| | AuNAs | CuNAs | CuLNAs |
|---|----------------------|----------------------|-----------------|
| Average diameter (TEM, nm) Shell thickness (TEM, nm) | 98±19 20.2±1.6 | 150±16 16.2±2.1 | 143±36 24±3 |
| Hydrodynamic diameter in PBS (DLS, nm) | 203.1±1.9 | 403±10 | 260.9±4.4 |
| Zeta potential in PBS (mV) | $^{-20.6}_{\pm 0.4}$ | $^{-15.2}_{\pm 0.7}$ | -21.6 ± 2.4 |
| Reference | [21] | [21] | this work |

investigate whether the nano-architectures treatments could modulate cancer cell invasiveness.

The anti-invasiveness potential of the nanoplatforms was evaluated employing a migration assay. To improve the reproducibility of the experiment, culture-insert 4-well plates were used. These plates permit an easy removal of the insert compared to traditional scratch assays, thus leaving a more regular and reproducible "scratch" on which cell migration can be monitored (Fig. 2b). Aiming to reduce the differences due to the insert geometry, the areas at different time points were normalized over the area at 24 h, meaning the free area immediately after the removal of the insert. A bigger free area is related to fewer invading cells, which is due to a reduced migratory tendency. As expected for NAs design, the effects of CuLNAs were visible 36 h after the treatment application, when the free area was significantly wider than the control (95 % and 80 % of the area at 24 h, respectively). In the following time points, the inhibition of cell migration became more evident, reaching the maximum between 48 h and 54 h (Fig. 2c). This tendency was transitory (reduced 72 h after the treatment) as suggested by NAs biodegradation kinetics [37]. In addition, copper homeostatic regulation in cancer cells could impact the time-dependent effect of CuLNAs. Indeed, the burst of Cu content from the complex may alter migratory tendency with an unknown mechanism until the homeostatic conditions are restored [42]. After 72 h, the exceeding Cu may be metabolized by cells, reducing the effect of the treatments. Overall, CuLNAs significantly reduced cell migration compared to AuNAs and CuNAs during the entire experimental window (Figure S2). We may speculate that CuL, as other reported copper(II) complexes, could intercalate DNA favoring the nucleophilic attack of oxydryl to the phosphodiester bonds in DNA, thus inducing DNA damage through the production of reactive oxygen species (ROS), consequently improving the outcome of Cu in CuLNAs [27,43]. These findings suggest that the antimigratory action on H4 cells is associated to CuL complex rather than the sole Cu ions. Moreover, the introduction of CuL inside AuNAs may reduce the systemic biodistribution of copper complex to healthy tissues according to the Enhanced Permeability and Retention (EPR) phenomenon of some carcinomas [44].

Nevertheless, the slowed cell migration induced upon CuLNAs treatment may be associated with a CuLNAs-induced cell proliferation that would eventually reflect on a slower wound healing. Indeed, the massive cell proliferation characterizing several cell subpopulations in the tumor mass leads to a mass growth that can eventually support the detachment of cells and their colonization in secondary body districts [45]. As a consequence, a reduced proliferation may correlate with slowed migration. For this reason, the effects of the different treatments on cell proliferation were evaluated to confirm whether the slower migration was due to NAs-induced slower proliferation rate (Figure S3). By counting the cells at 24 h, 48 h, and 72 h after the treatments, our results suggest that the antimigratory effect was not related to an impairment in cell proliferation. This supports the results of the viability assay, which were not altered by the nature of nanoparticles nor by any anti-proliferation tendency of the treatments [46]. AuNAs stimulated cell proliferation after 24 h, but this is not significative for the migration assay as the insert was removed after 24 h.

Taken together, these findings suggest that CuLNAs are more effective than AuNAs and CuNAs in impairing cell migration without affecting cell viability nor proliferation. To further confirm these observations, real time PCR experiments were conducted to investigate the expression of Epithelial-to-mesenchymal transition (EMT) related genes. In metastatic cancer cells, EMT supports migratory properties of cancer cells and allows invasion and colonization of secondary organs while conferring drug resistance and stemness to the tumor mass [10]. Cells lose their epithelial features and reduce the expression of proteins involved in cell-cell interaction, as E-cadherin. The motility can be acquired by overexpressing several mesenchymal traits, namely Snail, Vimentin, and Twist, which are strongly expressed by cancer cells experiencing EMT [47,48]. Moreover, Wnt signaling promotes EMT by

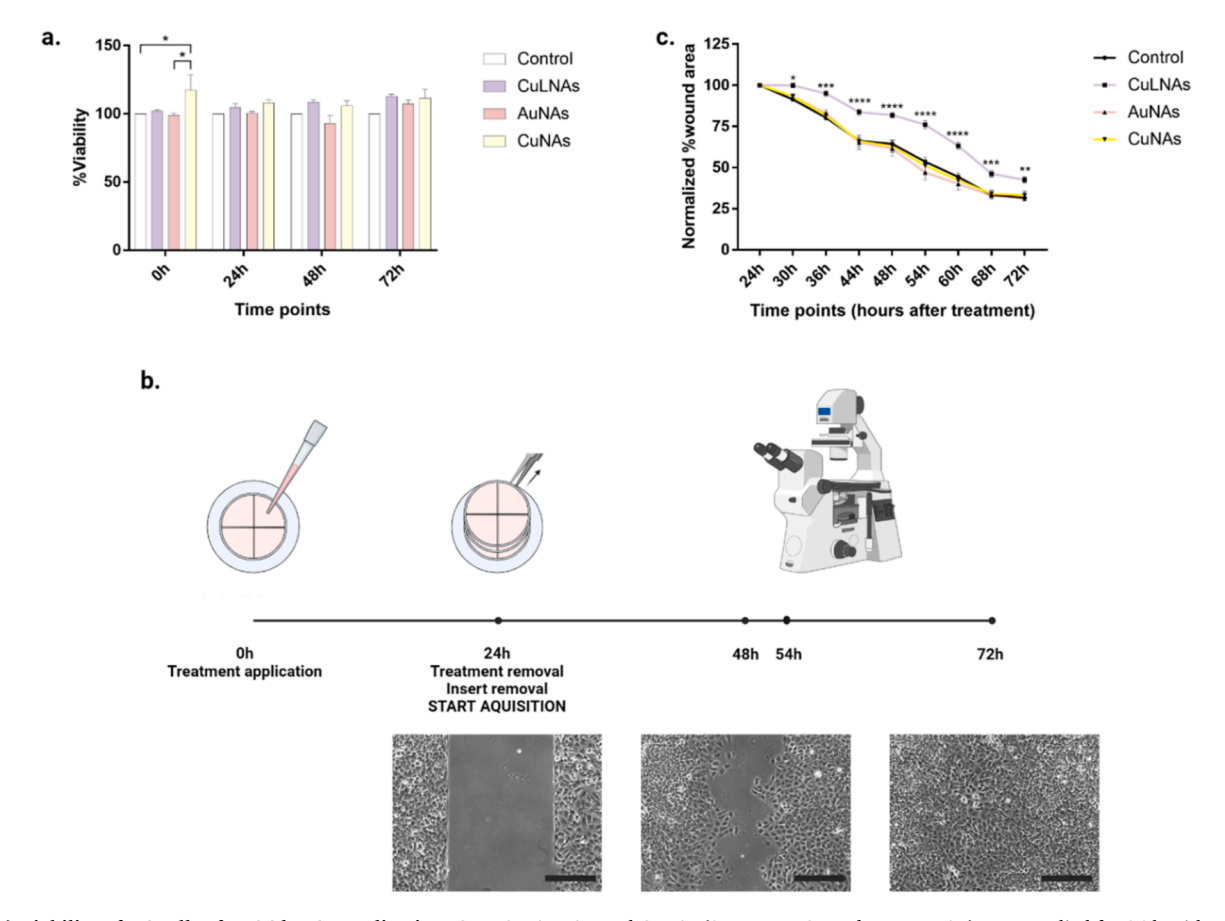


Fig. 2. (a) Viability of H4 cells after 24 h-NAs application. CuLNAs, AuNAs, and CuNAs ($0.5 \,\mu\text{g/mL}$ Cu and $5 \,\mu\text{g/mL}$ Au) were applied for 24 h without exerting toxicity. Viability was measured compared to the control represented by untreated cells. Data are reported as mean \pm standard error of the mean from two independent experiments performed in triplicate. Statistical analysis was performed using Two-way ANOVA with Tukey's multiple comparison test, *p<0.05 **p<0.01 ***p<0.001 ****p<0.0001. (b) Experimental settings of migration assay in 2D cultures of H4 cells. After the 24 h- administration of NAs, the insert was removed, and the wounds were monitored over time with an optical microscope to assess cell migration as %wound area. Scale bar: $500 \,\mu\text{m}$. (c) Normalized percentage of free wound area over time. The wound areas of the treatments were normalized over the respective area immediately after the insert removal. CuLNAs proved to significantly reduce cell migration starting from 36 h, with a maximum efficacy 54 h after treatment application. Data are reported as mean \pm standard error of the mean from three independent experiments performed in quadruplicate. Statistical analysis was performed against the control using Two-way ANOVA with Dunnett's multiple comparison test, *p<0.05 **p<0.01 ***p<0.001 ****p<0.0001.

inducing Snail, which is a transcriptional repressor of E-cadherin and a promoter of cell dissociation, and by activating the expression of MMP and c-Myc [3,49]. Considering our results on cell migration, we focused on the gene expression modulation 48 h, 54 h, and 72 h after the treatment application (Fig. 3). An anti-invasiveness approach would stimulate the overexpression of E-cadherin encoding gene, while downregulating the expression of mesenchymal proteins and transcriptional factors. Confirming our previous findings, CuLNAs effect on the EMT-related genes was visible 48 h after the treatment administration, reached the peak at 54 h and disappeared after 72 h, concomitantly with complete NAs degradation. Given the significative anti-migratory effect observed at 54 h, the expression of additional EMT-related genes was evaluated for this time point (Fig. 3c). We focused on mesenchymal genes expressing for N-cadherin, MMP2, and MMP9, along with EMT transcriptional factors Zeb1 and Slug [10]. The investigation was extended to c-Myc, a proto-oncogene associated with several types of cancers, and the gene encoding for superoxide dismutase 1 (SOD1) [50]. SOD1 was evaluated as it is a Cu²⁺/Zn²⁺ enzyme involved in the metastatic development, and its reduced expression is associated with better prognosis [51]. At 54 h, E-cadherin encoding gene was upregulated by all tested NAs, corroborating the anti-migratory tendency recognized for CuLNAs in the migration assay on H4 cells. On the other hand, NAs downregulated the expression of Snail, Twist, Vimentin- and MMPs-encoding genes. Thus, the mild downregulation of mesenchymal

genes induced by CuLNAs reinforced the antimetastatic behavior of AuNAs due to the loaded CuL.

Overall, the introduction of a copper complex within AuNAs results in a macroscopic effect on the invasiveness of glioma cancer cells, and at the same time, the combination of CuL and Au USNPs improves the effect of the sole copper ions provided by CuNAs.

5. Conclusion

CuL has been successfully loaded into ultrasmall-in-nano architectures, confirming the versatility of the production SOPs. The quantitative biological data demonstrate that CuLNAs have an increased antiinvasiveness efficacy on gliomas compared to both AuNAs and CuNAs. Nevertheless, these results are exploratory and further investigations are required to confirm the antimetastatic tendency of CuLNAs, especially with more advanced models, such as 3D spheroids and chorioallantoic membrane (CAM) assay [52]. It should be noted that an interesting behavior of NAs is the transient biodistribution to the brain (without metal persistence) following intranasal instillation [38]. This behavior may be exploited for future investigations aiming at delivering CuL to the brain to localize its action over glioma recurrence and cerebral metastases. Moreover, the already reported radiosensitizing effect of Au nanoparticles may emphasize the migration inhibition induced by a CuL analogue after radiotherapy, reducing relapses [23,41]. Overall, these

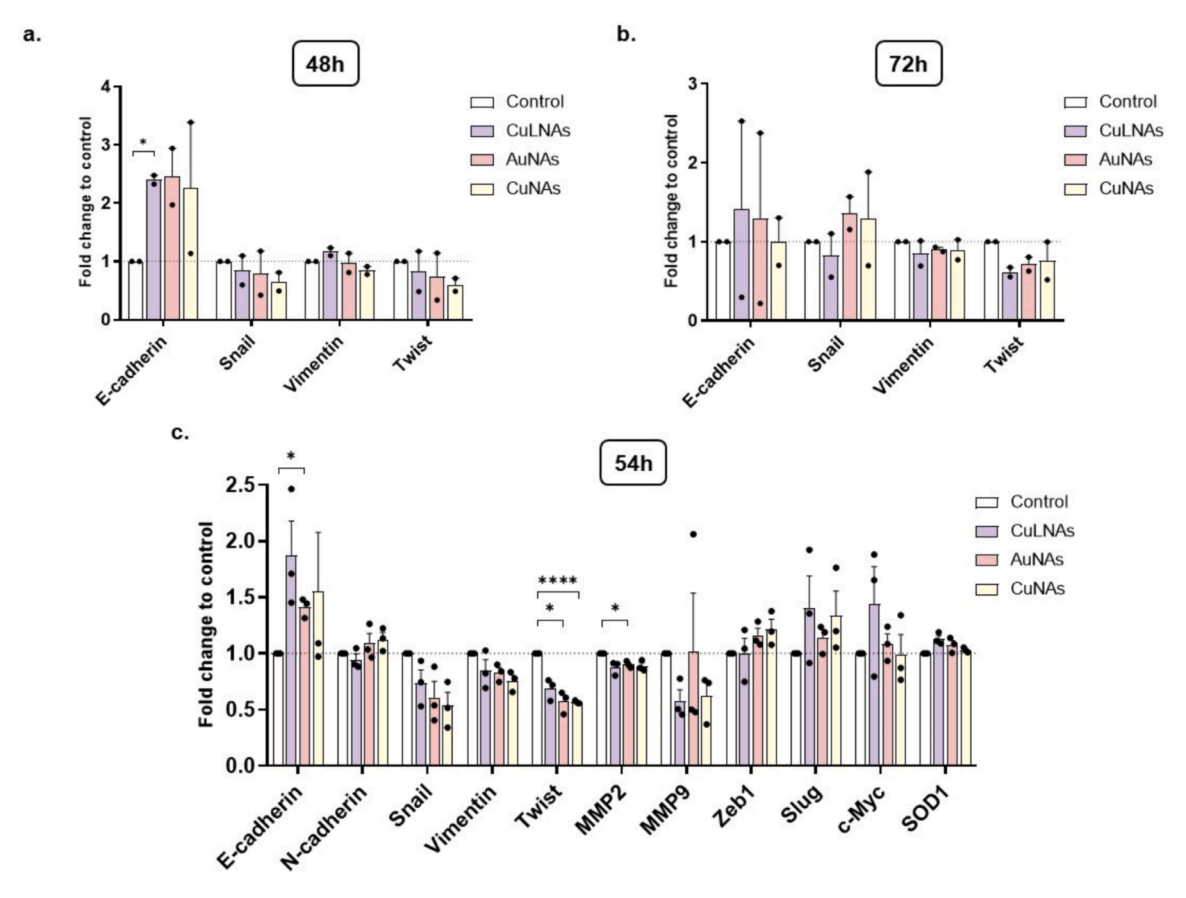


Fig. 3. Expression of EMT-related genes after NAs application. CuLNAs reduced migration inhibiting Epithelial-to-Mesenchymal transition (EMT) in H4 glioma cells after 48 h (a), 54 h (c), and 72 h (b). The effect began 48 h after the treatment application and reached the maximum after 54 h. In agreement to migration results, the regulation of EMT-related genes ceased after 72 h. The results were calculated from two (a and b) or three (c) independent results, and the results are provided as mean \pm standard error of the mean. Statistical significance was calculated using multiple t test with Holm-Sidak's multiple comparison test, *p<0.05, **p<0.01, ***p<0.001, ***p<0.001, ***p<0.0001.

results support future efforts toward the establishment of a family of NAs-based anti-metastasis agents for gliomas.

6. CRediT authorship contribution statement

Luca Tirinato: Formal analysis. Agata Zamborlin: Writing – original draft, Investigation, Data curation, Conceptualization. Francesca Pagliari: Methodology, Investigation, Data curation. Maria Ermini: Investigation, Formal analysis. Valentina Frusca: Investigation, Formal analysis. Giulio Bresciani: Investigation. Fabio Marchetti: Writing – review & editing, Validation, Supervision, Formal analysis. Joao Seco: Writing – review & editing, Writing – original draft, Validation, Supervision. Valerio Voliani: Writing – review & editing, Writing – original draft, Validation, Supervision. Stefania Volante: Investigation. Daniel García-Calderón: Data curation.

Declaration of Competing Interest

The Authors declare no competing financial interests that could have appeared to influence the work reported in this paper.

Data Availability

Data will be made available on request.

Acknowledgments

Figures were created with BioRender.com.

Authors' contribution

A.Z., F.P., M.L.E., V.F., D.A.G.C., S.V., G.B., F.M., investigation; D.A. G.C., software; A.Z., F.P., V.F., formal analysis; A.Z., visualization; V.V., J.S., L.T., conceptualization; V.V., J.S., F.M., resources and supervision; . All Authors have discussed the data and contributed to write the manuscript.

Appendix A. Supporting information

Supplementary data associated with this article can be found in the online version at doi:10.1016/j.colsurfb.2024.114187.

References

- [1] Q.T. Ostrom, M. Price, C. Neff, G. Cioffi, K.A. Waite, C. Kruchko, J.S. Barnholtz-Sloan, CBTRUS statistical report: primary brain and other central nervous system tumors diagnosed in the United States in 2015-2019, Neuro. Oncol. 24 (5) (2022) v1–v95.
- [2] K.D. Miller, Q.T. Ostrom, Brain and other central nervous system tumor statistics, Ca. Cancer J. Clin. 71 (2021) 381–406.
- [3] I. Paw, R.C. Carpenter, K. Watabe, W. Debinski, H.W. Lo, Mechanisms regulating glioma invasion, Cancer Lett. 362 (1) (2015) 1–7.
- [4] M. Weller, M. van den Bent, M. Preusser, E. Le Rhun, J.C. Tonn, G. Minniti, M. Bendszus, C. Balana, O. Chinot, L. Dirven, P. French, M.E. Hegi, A.S. Jakola, M. Platten, P. Roth, R. Rudà, S. Short, M. Smits, M.J.B. Taphoorn, A. von Deimling, M. Westphal, R. Soffietti, G. Reifenberger, W. Wick, EANO guidelines on the diagnosis and treatment of diffuse gliomas of adulthood, Nat. Rev. Clin. Oncol. 18 (3) (2021) 170–186.
- [5] M. Weller, W. Wick, K. Aldape, M. Brada, M. Berger, S.M. Pfister, R. Nishikawa, M. Rosenthal, P.Y. Wen, R. Stupp, G. Reifenberger, et al., Nat. Rev. Dis. Prim. 1 (2015) 15017.

- [6] Q. Sun, R. Xu, H. Xu, G. Wang, X. Shen, H. Jiang, Extracranial metastases of high-grade glioma: the clinical characteristics and mechanism, World J. Surg. Oncol. 15 (2017) 81
- [7] P. Beauchesne, Extra-neural metastases of malignant gliomas: myth or reality? Cancers (Basel) 3 (2011) 461–477.
- [8] T. Meirson, H. Gil-Henn, A.O. Samson, Invasion and metastasis: the elusive hallmark of cancer, Oncogene 39 (9) (2020) 2024–2026.
- [9] X.T. Qi, J.S. Zhan, L.M. Xiao, L. Li, H.X. Xu, Z.B. Fu, The unwanted cell migration in the brain: glioma metastasis, Neurochem. Res. 42 (2017) 1847–1863.
- [10] A. Zamborlin, V. Voliani, Gold nanoparticles as antiangiogenic and antimetastatic agents, Drug Discov. Today 28 (2) (2022) 103438.
- [11] J. Zhang, N. Wang, Q. Li, Y. Zhou, Y. Luan, A two-pronged photodynamic nanodrug to prevent metastasis of basal-like breast cancer, Chem. Commun. 57 (18) (2021) 2305–2308.
- [12] A. Dev, M.N. Sardoiwala, M. Boddu, S.J. Mohanbhai, S.R. Choudhury, S. Karmakar, 4-oxo-fenretinide-loaded human serum albumin nanoparticles for the inhibition of epithelial-mesenchymal transition in neuroblastoma xenografts, ACS Appl. Nano Mater. 5 (5) (2022) 7540–7548.
- [13] Y. Huang, W. Hong, X. Wei, The molecular mechanisms and therapeutic strategies of EMT in tumor progression and metastasis, J. Hematol. Oncol. 15 (1) (2022) 1–27.
- [14] S. Jonckheere, J. Adams, D. De Groote, K. Campbell, G. Berx, S. Goossens, Epithelial-mesenchymal transition (EMT) as a therapeutic target, Cells Tissues Organs 211 (2) (2022) 157–182.
- [15] V. Mittal, Epithelial mesenchymal transition in tumor metastasis, Annu. Rev. Pathol. Mech. Dis. 13 (2018) 395–412.
- [16] N. Pandey, P. Anastasiadis, C.P. Carney, P.P. Kanvinde, G.F. Woodworth, J. A. Winkles, A.J. Kim, Nanotherapeutic treatment of the invasive glioblastoma tumor microenvironment, Adv. Drug Deliv. Rev. 188 (2022) 114415.
- [17] J.F. Guerreiro, M.A.G.B. Gomes, F. Pagliari, J. Jansen, M.G. Marafioti, C. Nistico, R. Hanley, R.O. Costa, S.S. Ferreira, F. Mendes, C. Fernandes, A. Horn, L. Tirinato, J. Seco, Iron and copper complexes with antioxidant activity as inhibitors of the metastatic potential of glioma cells, RSC Adv. 10 (22) (2020) 12699–12710.
- [18] X. Shi, Z. Chen, Y. Wang, Z. Guo, X. Wang, Hypotoxic copper complexes with potent anti-metastatic and anti-angiogenic activities against cancer cells, Dalt. Trans. 47 (14) (2018) 5049–5054.
- [19] D.A. da Silva, A. De Luca, R. Squitti, M. Rongioletti, L. Rossi, C.M.L. Machado, G. Cerchiaro, Copper in tumors and the use of copper-based compounds in cancer treatment, J. Inorg, Biochem. 226 (July 2021) (2022) 111634.
- [20] S. Tsymbal, G. Li, N. Agadzhanian, Y. Sun, J. Zhang, M. Dukhinova, V. Fedorov, M. Shevtsov, Recent advances in copper-based organic complexes and nanoparticles for tumor theranostics, Molecules 27 (2022) 7066.
- [21] A. Zamborlin, P. Sarogni, V. Frusca, A. Gonnelli, N. Giannini, M.L. Ermini, A. Marranci, F. Pagliari, C.M. Mazzanti, J. Seco, V. Voliani, Drug-free hybrid nanoarchitectures modulate the metastatic behavior of pancreatic ductal adenocarcinoma in alternative in vivo models, ACS Appl. Nano Mater. 6 (24) (2023) 22532-22544.
- [22] Valentina Frusca, Chiara Cavallini, Agata Zamborlin, Giuliana Drava, Virginia Barone, Lisa Gherardini, Mario Chiarello, Paolo Armanetti, Maria Laura Ermini, Luca Menichetti, Valerio Voliani, In vivo combined photoacoustic imaging and photothermal treatment of HPV-negative head and neck carcinoma with NIRresponsive non-persistent plasmon nano-architecture, Advanced Therapeutics (2024), https://doi.org/10.1002/adtp.202400110.
- [23] Alessandra Gonnelli, Marine Gerbé de Thoré, Maria Laura Ermini, Valentina Frusca, Agata Zamborlin, Nicolas Signolle, Olivia Bawa, Céline Clémenson, Lydia Meziani, Paul Bergeron, Ismail El-Azrak, Patrizia Sarogni, Enrico Mugnaioli, Noemi Giannini, Giuliana Drava, Eric Deutsch, Fabiola Paiar, Michele Mondini, Valerio Voliani, Nonpersistent nanoarchitectures enhance concurrent chemoradiotherapy in an immunocompetent orthotopic model of. HPV + head/neck carcinoma, Advanced Materials (2024), https://doi.org/10.1002/ adma.202400949.
- [24] A. Neves, C.N. Verani, M.A. De Brito, I. Vencato, A. Mangrich, G. Oliva, D.D.H. F. Souza, A.A. Batista, Copper(II) complexes with (2-Hydroxybenzyl-2-Pyridylmethyl)amine-Hbpa: syntheses, characterization and crystal structures of the ligand and [Cu(II)(Hbpa)2](ClO4)2·2H2O, Inorg. Chim. Acta 290 (2) (1999) 207–212.
- [25] A.Z. Halimehjani, S.E. Hooshmand, E.V. Shamiri, Synthesis of α-phthalimido-A'-dithiocarbamato propan-2-Ols via a one-pot, three-component epoxide ring-opening in water, Tetrahedron Lett. 55 (40) (2014) 5454–5457.
- [26] Menges, F. Spectragryph Optical Spectroscopy Software, Version 1.2.16d, @ 2016-2020, Https://Www.Effemm2.de/Spectragryph.
- [27] A.J. Horn, I. Vencato, A.J. Bortoluzzi, R. Hörner, R.A.N. Silva, B. Spoganicz, V. Drago, H. Terenzi, M.C.B. De Oliveira, R. Werner, W. Haase, A. Neves, Synthesis, crystal structure and properties of dinuclear iron(III) complexes containing terminally coordinated phenolate/H2O/OH groups as models for purple acid phosphatases: efficient hydrolytic DNA cleavage, Inorg. Chim. Acta 358 (2) (2005) 339–351.
- [28] J. Seco, J.F. Guerreiro, M. Gomes, A. Horn, C.F. Horn, F. Pagliari, Compound for preventing migration of cancer cells, US Pat. Appl. 17 (766) (2022) 128.

- [29] Seco, J.; Guerreiro, J.F.; Guimaraes Barbosa Gomes, M. A.; Horn Junior, A.; Horn, C. F. WO 2021/064175 A1, 2021.
- [30] M.L. Ermini, M. Summa, A. Zamborlin, V. Frusca, A.K. Mapanao, E. Mugnaioli, R. Bertorelli, V. Voliani, Copper nano-architectures topical cream for the accelerated recovery of burnt skin, Nanoscale Adv. 5 (4) (2023) 1212–1219.
- [31] K.J. Livak, T.D. Schmittgen, Analysis of relative gene expression data using realtime quantitative PCR and the 2-ΔΔCT method, Methods 25 (4) (2001) 402–408.
- [32] M. Bortoluzzi, G. Bresciani, F. Marchetti, G. Pampaloni, S. Zacchini, Synthesis and structural characterization of mixed halide–N,N-diethylcarbamates of group 4 metals, including a case of unusual tetrahydrofuran activation, N. J. Chem. 41 (4) (2017) 1781–1789.
- [33] L. Biancalana, G. Bresciani, C. Chiappe, F. Marchetti, G. Pampaloni, C.S. Pomelli, Modifying bis(Triflimide) ionic liquids by dissolving early transition metal carbamates, Phys. Chem. Chem. Phys. 20 (7) (2018) 5057–5066.
- [34] L.J.H. Borges, É.S. Bull, C. Fernandes, A. Horn, N.F. Azeredo, J.A.L.C. Resende, W. R. Freitas, E.C.Q. Carvalho, L.S. Lemos, H. Jerdy, M.M. Kanashiro, In vitro and in vivo studies of the antineoplastic activity of copper (ii) compounds against human leukemia THP-1 and murine melanoma B16-F10 cell lines, Eur. J. Med. Chem. 123 (2016) 128–140.
- [35] D. Liu, F. Yang, F. Xiong, N. Gu, The smart drug delivery system and its clinical potential, Theranostics 6 (9) (2016) 1306–1323.
- [36] Patrizia Sarogni, Valentina Frusca, Agata Zamborlin, Noemi Giannini, Menicagli Michele, Luigi Brancato, Stefania Linsalata, Fabio Di Martino, Alessandra Gonnelli, Fabiola Paiar, Johan Van den Bossche, Johannes Bogers, Valerio Voliani, Neoadjuvant hyperthermia combined with hybrid nanoarchitectures enhances chemoradiotherapy efficacy in head and neck carcinoma, ACS Applied Materials and Interfaces (2024), https://doi.org/10.1021/ acsami.4c07393.
- [37] D. Cassano, A. Mapanao, M. Summa, Y. Vlamidis, G. Giannone, M. Santi, E. Guzzolino, L. Pitto, L. Poliseno, R. Bertorelli, V. Voliani, Biosafety and biokinetics of noble metals: the impact of their chemical nature, ACS Appl. Bio Mater. 2 (10) (2019) 4464–4470.
- [38] A.K. Mapanao, G. Giannone, M. Summa, M.L. Ermini, A. Zamborlin, M. Santi, D. Cassano, R. Bertorelli, V. Voliani, Biokinetics and clearance of inhaled gold ultrasmall-in-nano architectures, Nanoscale Adv. 2 (2020) 3815–3820.
- [39] A. Zamborlin, M.L. Ermini, M. Summa, G. Giannone, V. Frusca, A.K. Mapanao, D. Debellis, R. Bertorelli, V. Voliani, The fate of intranasally instilled silver nanoarchitectures, Nano Lett. 22 (2022) 5269–5276.
- [40] M. Santi, V. Frusca, M.L. Ermini, A.K. Mapanao, P. Sarogni, A. Gonnelli, N. Giannini, A. Zamborlin, L. Biancalana, F. Marchetti, V. Voliani, Hybrid nanoarchitectures loaded with metal complexes for the co-chemotherapy, J. Mater. Chem. B 11 (2) (2023) 325–334.
- [41] Gonnelli Alessandra, Patrizia Sarogni, Giannini Noemi, Stefania Linsalata, Fabio Di Martino, Zamborlin Agata, Valentina Frusca, Ermini Maria Laura, Puccini Paola, Voliani Valerio, Paiar Fabiola, A bioconvergence study on platinum-free concurrent chemoradiotherapy for the treatment of HPV-negative head and neck carcinoma, Artificial cells, nanomedicine and biotechnology 52 (1) (2024) 122–129, https://doi.org/10.1080/21691401.2024.2309233.
- [42] P. Lelièvre, L. Sancey, J.L. Coll, A. Deniaud, B. Busser, The multifaceted roles of copper in cancer: a trace metal element with dysregulated metabolism, but also a target or a bullet for therapy, Cancers (Basel) 12 (12) (2020) 1–25.
- [43] C. Liu, J. Zhou, Q. Li, L. Wang, Z. Liao, H. Xu, DNA damage by copper(ii) complexes: coordination-structural dependence of reactivities, J. Inorg. Biochem. 75 (3) (1999) 233–240.
- [44] H. Maeda, J. Wu, T. Sawa, Y. Matsumura, K. Hori, Tumor vascular permeability and the epr effect in macromolecular therapeutics: a review, J. Control. Release 65 (1–2) (2000) 217–284.
- [45] J.A. Gallaher, J.S. Brown, A.R.A. Anderson, The Impact of proliferation-migration tradeoffs on phenotypic evolution in cancer, Sci. Rep. 9 (1) (2019) 1–10.
- [46] S.N. Rampersad, Multiple applications of alamar blue as an indicator of metabolic function and cellular health in cell viability bioassays, Sensors 12 (9) (2012) 12347–12360.
- [47] N.M. Aiello, Y. Kang, Context-dependent EMT programs in cancer metastasis, J. Exp. Med. 216 (5) (2019) 1016–1026.
- [48] I. Pastushenko, C. Blanpain, EMT transition states during tumor progression and metastasis, Trends Cell Biol. 29 (3) (2019) 212–226.
- [49] C. Boccaccio, P.M. Comoglio, Invasive growth: a MET-driven genetic programme for cancer and stem cells, Nat. Rev. Cancer 6 (August) (2006) 30–32.
- [50] J.W. Herms, F.D. Von Loewenich, J. Behnke, E. Markakis, H.A. Kretzschmar, C-Myc oncogene family expression in glioblastoma and survival, Surg. Neurol. 51 (5) (1999) 536–542.
- [51] M.L. Gomez, N. Shah, T.C. Kenny, E.C. Jenkins, D. Germain, SOD1 Is essential for oncogene-driven mammary tumor formation but dispensable for normal development and proliferation, Oncogene 38 (29) (2019) 5751–5765.
- [52] A.K. Mapanao, P.P. Che, P. Sarogni, P. Sminia, E. Giovannetti, V. Voliani, Tumor Grafted-chick chorioallantoic membrane as an alternative model for biological cancer research and conventional/nanomaterial-based theranostics evaluation, Expert Opin. Drug Metab. Toxicol. 17 (8) (2021) 947–968.